Flavin containing monooxygenase 2 regulates renal tubular cell fibrosis and paracrine secretion via SMURF2 in AKI-CKD transformation

LONGFEI WANG[1*], HONGCHU ZHA[2*], JING HUANG[3] and LANG SHI[2,3]

[1]Children's Hospital Affiliated to Zhengzhou University, Henan International Joint Laboratory of Prevention and Treatment of Pediatric Diseases, Henan Children's Hospital, Zhengzhou Children's Hospital, Zhengzhou, Henan 450018; [2]Department of Nephrology, The First Clinical Medical College of Three Gorges University, Center People's Hospital of Yichang, Kidney Disease Research Institute of China Three Gorges University, Yichang, Hubei 443000; [3]Department of Nephrology, Renmin Hospital of Wuhan University, Wuhan, Hubei 430060, P.R. China

Received June 30, 2023; Accepted September 22, 2023

DOI: 10.3892/ijmm.2023.5313

Abstract. In the follow-up of hospitalized patients with acute kidney injury (AKI), it has been observed that 15-30% of these patients progress to develop chronic kidney disease (CKD). Impaired adaptive repair of the kidneys following AKI is a fundamental pathophysiological mechanism underlying renal fibrosis and the progression to CKD. Deficient repair of proximal tubular epithelial cells is a key factor in the progression from AKI to CKD. However, the molecular mechanisms involved in the regulation of fibrotic factor paracrine secretion by injured tubular cells remain incompletely understood. Transcriptome analysis and an ischemia-reperfusion injury (IRI) model were used to identify the contribution of flavin-containing monooxygenase 2 (FMO2) in AKI-CKD. Lentivirus-mediated overexpression of FMO2 was performed in mice. Functional experiments were conducted using TGF-β-induced tubular cell fibrogenesis and paracrine pro-fibrotic factor secretion. Expression of FMO2 attenuated kidney injury induced by renal IRI, renal fibrosis, and immune cell infiltration into the kidneys. Overexpression of FMO2 not only effectively blocked TGF secretion in tubular cell fibrogenesis but also inhibited aberrant paracrine activation of pro-fibrotic factors present in fibroblasts. FMO2 negatively regulated TGF-β-mediated SMAD2/3 activation by promoting the expression of SMAD ubiquitination regulatory factor 2 (SMURF2) and its nuclear translocation. During the transition from AKI to CKD, FMO2 modulated tubular cell fibrogenesis and paracrine secretion through SMURF2, thereby affecting the outcome of the disease.

Correspondence to: Dr Lang Shi, Department of Nephrology, Renmin Hospital of Wuhan University, 238 Donghu Road, Wuchang, Wuhan, Hubei 430060, P.R. China
E-mail: langshi@whu.edu.cn

*Contributed equally

Key words: FMO2, acute kidney injury, ischemia-reperfusion injury, chronic kidney disease, renal fibrosis

Introduction

Acute kidney injury (AKI) refers to a clinical syndrome characterized by a sudden and severe decline in kidney function, resulting from various factors. Due to its high incidence and mortality rates, AKI has become a global clinical problem (1,2). Despite certain advancements in the prevention and treatment of this disease, a significant proportion of patients who recover from AKI exhibit reduced kidney function and progress to develop chronic kidney disease (CKD), including end-stage renal disease (3-5). Follow-up studies of hospitalized patients with AKI have shown that 15-30% of them progress to CKD (6-8). Tubulointerstitial fibrosis (TIF) is a typical pathological feature of CKD, and its extent serves as a marker for predicting CKD progression (9). The occurrence and development of TIF involves complex processes with the participation of multiple cell types, with a particular focus on fibroblasts that produce a large quantity of extracellular matrix (ECM) components upon activation. However, increasing evidence has demonstrated the significance of the contribution of renal tubular cells in TIF. Severe AKI injuries lead to abnormal repair of tubular cells, resulting in the production and secretion of various cytokines, growth factors, pro-inflammatory molecules, and pro-fibrotic molecules (10). The increased bioactive molecules play a role in both autocrine function, which is necessary for the de-differentiation, migration, and proliferation of tubular cells during regeneration (10,11), and in normal paracrine function, for recruiting leukocytes from circulation and activating fibroblasts and other interstitial cells (11,12). The characteristics of activated fibroblasts include elevated expression of contractile proteins, increased cell motility, induction of pro-inflammatory genes, and high-level deposition of collagen and other ECM proteins (13). TGF-β and the phosphorylated form of SMAD2/3, which acts downstream in the signaling pathway, are crucial intracellular

signals in fibroblast activation, including renal myofibroblast activation (14-16). However, the molecular mechanisms underlying the dysregulated paracrine secretion of fibrotic factors by injured tubular cells remain incompletely understood. Therefore, a thorough investigation of the mechanisms leading to kidney fibrosis following AKI and the identification of potential intervention targets are crucial for preventing the chronic progression of AKI.

In the current study, the transcriptomic dataset of kidney tissues following ischemia-reperfusion injury [IRI; gene expression omnibus (GEO) dataset GSE98622] was analyzed (17). The data indicated dynamic changes in the expression of the flavin-containing monooxygenase (FMO) family between 2 h and 14 days post-ischemia reperfusion. A recent study has identified that FMO2 possesses a previously uncharacterized enzyme-independent antifibrotic activity via the cytochrome P450 2J3-SMAD ubiquitination regulatory factor 2 (SMURF2) axis (18). Particularly, FMO1 and FMO2, which are abundantly expressed in the kidney, are of significant interest. FMOs are a class of enzymes that utilize flavin coenzymes to introduce a single oxygen atom into chemical reactions. These enzymes interact with oxygen molecules, transferring the oxygen atom to substrates and undergoing oxidation-reduction reactions. They typically function in conjunction with reducing agents, such as coenzymes NADH or flavin adenine dinucleotide, to provide the necessary electrons for the reactions (19). FMOs play various roles in biological systems. FMO2 is primarily expressed in human lungs, followed by the kidneys, and exhibits high activity during infancy. It participates in the metabolism of exogenous compounds, including certain drugs and environmental toxins, such as sulfur-containing compounds (20). IRI triggers an inflammatory response and members of the FMO family may be involved in regulating the inflammation processes induced by IRI. These enzymes may impact the intensity and duration of the inflammatory response by modulating the synthesis and metabolism processes of inflammatory mediators, such as leukocyte activation, cytokine production, and cell adhesion molecule expression (21,22). It has been shown in a previous study conducted by our research group that renal expression of FMO2 mitigates post-AKI functional impairment and immune cell infiltration into the kidneys. Furthermore, members of the FMO family may participate in tubular cell-mediated paracrine secretion of pro-fibrotic factors, thereby influencing the fibrotic process. It is important to note that FMO2 overexpression inhibits the effects of TGF-β and the phosphorylation of SMAD2/3. FMO2 expression negatively regulates the TGF-β signaling pathway through the induction of SMURF2 expression and its nuclear translocation. SMURF2 serves as an intrinsic negative regulator of SMAD2/3 phosphorylation and of the TGF-β1 signaling pathway. Therefore, the present study demonstrated that FMO2 acted as an inhibitor of the TGF-β/SMAD2/3 signaling pathway, exerting a conservative ameliorative effect on renal fibrosis and pathological remodeling. However, the specific mechanisms and effects may vary depending on the type of fibrosis and tissue specificity. Further investigations will contribute to a deeper understanding of the specific roles of the FMO family in the process of renal fibrosis, thereby providing new targets for the treatment of this disease.

Materials and methods

Transcriptomic profiling and differential expression analysis of a murine renal bilateral ischemia-reperfusion mode. The GSE98622 (17) mRNA expression profile dataset was downloaded from GEO (https://www.ncbi.nlm.nih.gov/geo/). The 'limma' software package helped identify differentially expressed genes. The 'heatmap' software packages of R software were used to draw heat maps.

Experimental animals for renal ischemia-reperfusion injury. Male C57BL/6 mice weighing 20-25 g were purchased from the Experimental Animal Center of China Three Gorges University (Yichang, China) and maintained under specific pathogen-free conditions. All animal experiments were conducted in accordance with the regulations of the relevant laws and approved by the Ethics Committee of the Children's Hospital Affiliated to Zhengzhou University (approval no. 2023-K-074).

Unilateral renal ischemia/reperfusion model. Unilateral ischemic acute kidney injury (AKI) or chronic kidney disease (CKD) mouse models were established by clamping the left renal artery. Unilateral renal ischemia-reperfusion was performed as recently described (7,11). Briefly, mice were anesthetized by intraperitoneal injection of pentobarbital (60 mg/kg) prior to surgery. The left renal artery was isolated, and a microaneurysm clip was used to clamp the artery for 28 min, inducing renal ischemia-reperfusion injury. After 28 min, blood flow was restored by releasing the clamp, and the layers of muscle and skin were sutured sequentially. Throughout the entire surgical procedure, the mice were maintained at a body temperature of 36-37.2˚C. One day before euthanasia, the non-clamped right kidney was removed. Following a reperfusion period of either 24 h or 14 days, mice were euthanized through cervical dislocation under inhalation anesthesia using 3% isoflurane, and serum and kidney tissue samples were collected. The control group underwent a sham operation without clamping the renal artery.

Cell culture. Boston University mouse proximal tubule cells (BUMPT; obtained from Dr Lieberthal and Dr Shwartz at Boston University) were cultured in DMEM (Dulbecco's modified Eagle's medium) (Thermo Fisher Scientific, Inc.) with 10% fetal bovine serum, penicillin (100 U/ml) and streptomycin (100 μg/ml) in a humidified atmosphere of 5% CO_2 at 37˚C. NRK-49F rat kidney interstitial fibroblast cells were obtained from the American Type Culture Collection. Cells were cultured in Dulbecco's modified Eagle's medium/nutrient mixture F-12 (DMEM/F-12) medium supplemented with 10% fetal bovine serum (Invitrogen; Thermo Fisher Scientific, Inc.).

Gene delivery in vivo. In the animal study, 10 days prior to renal ischemia, the recombinant lentiviral vector PGLV carrying FMO2 (Shanghai GenePharma, Co., Ltd.) was introduced into the mouse left kidney as previously described (7,23). Briefly, mice were anesthetized by intraperitoneal injection of pentobarbital (60 mg/kg) prior to surgery (24). A total of 100 μl lentivirus solution [1x10^5 transduction units (TU)/μl] was injected into anesthetized mice with a 30 G syringe. The

needle was inserted from the lower pole to the upper pole of the kidney, and the lentivirus solution was slowly injected while withdrawing the needle.

Treatment of renal tubule cells with TGF-β. BUMPT cells reached ~60% confluence, they were exposed to serum-free DMEM supplemented with 10 ng/ml recombinant human TGF-β for 48 h. Control cells were cultured in serum-free medium without TGF-β. At specified time points, cells were collected for analysis of mRNA and protein levels to detect fibrogenic factors such as Vimentin, actin α 2, smooth muscle (Acta2), platelet-derived growth factor subunit B (Pdgfb) and cellular communication network factor 2 (Ccn2).

Collection of renal tubule conditioned media and intervention on renal fibroblasts (NRK-49F). For renal tubule cells, cells were seeded in 60 mm culture dishes at a density of $1x10^6$ cells/dish for BUMPT cells. When cells reached ~60% confluence, they were treated with 10 ng/ml TGF-β in serum-free DMEM for 48 h, while control cells were maintained in serum-free medium without TGF-β for 48 h. Subsequently, the medium for both TGF-β-treated cells and control cells was replaced with complete medium without TGF-β, and further incubated for 24 h to collect renal tubule cells-conditioned media. The tubular cell-conditioned media were concentrated using Amicon® Ultra-4 centrifugal filter devices (cat. no. UFC8003; MilliporeSigma) with a molecular weight cutoff of 3 kDa. A total of 4 ml of conditioned media were collected from each 60 mm culture dish, and the supernatant was transferred to the Milli-Q® water pre-rinsed centrifugal filter device. It was then centrifuged at 7,500 x g for 1 h at 4˚C using a fixed-angle rotor to recover ~100 μl concentrated conditioned media.

To treat fibroblasts with renal tubule cell-conditioned media, NRK-49F fibroblasts were seeded in 12-well plates at a density of $0.15x10^6$ cells/well and reached ~80% confluence on the following day. After overnight serum starvation in serum-free DMEM, NRK-49F fibroblasts were incubated with renal tubule cell-conditioned media (diluted 100 μl in 1 ml serum-free DMEM) for 48 h. Cell morphology was monitored, and cells were counted using the Bio-Rad TC20 automated cell counter (Bio-Rad Laboratories, Inc.) after trypsin digestion. Subsequently, cells were lysed for measurement of cellular protein and immunoblot analysis. In experiments testing the effects of fibroblast growth factor 2 (FGF2) and antibodies, antibodies or mouse IgG were pre-incubated with renal tubule cell-conditioned media at room temperature for 1.5 h before adding them to NRK-49F fibroblasts.

Histology, immunohistochemistry, immunofluorescence and TUNEL staining. Tissues were transferred to 4% paraformaldehyde and fixed by leaving tissues at 4˚C overnight, then embedded in paraffin and cross-sectioned (4 μm) for histology examination. H&E and Masson's trichrome were performed according to manufacturer's instructions (Beijing Solarbio). Immunohistochemistry and immunofluorescence techniques were employed using 5 μm sections of mouse kidney tissues. Antigen retrieval was performed using 10 mM sodium citrate, pH 6.0, 0.05% Tween (0.1 mmol sodium citrate in 5 ml + dH_2O 45 ml + Tween X 100 25 μl; 100 mM sodium citrate stored at 4˚C). Samples were boiled in the above buffer in a steamer for 60 min and then allowed to cool at room temperature for 20 min. The slides were washed with PBS and blocked with blocking buffer [1% bovine serum albumin (BSA), 1% goat serum, 0.3% Triton X-100 in PBS] for 20-40 min at room temperature. After antigen retrieval and blocking, primary antibodies against FMO2 (cat. no. NBP1-85952; Novus Biologicals, LLC; 1:500 dilution), Kim-1 (cat. no. AF1750; R&D Systems, Inc.; 1:200 dilution), macrophage (F4/80) (cat. no. ab56297; Abcam; 1:50 dilution), myeloperoxidase (MPO; cat. no. MAK283; MilliporeSigma; 1:200 dilution), α-SMA (cat. no. ab5694; Abcam; 1:200 dilution) and Vimentin (cat. no. ab92547; Abcam; 1:200 dilution) were used to detect specific markers incubating at 4˚C overnight. For immunohistochemistry, sections were initially washed thrice with PBS before 1-h incubation at 37˚C with an HRP-labeled secondary antibody. Diaminobenzidine tetrahydrochloride served as the enzyme substrate for visualization, followed by hematoxylin counterstaining. Images were then acquired using cellSens software (V3.2; cellSens) at x200 magnification. For tissue immunofluorescence, samples were incubated for 1 h at 25˚C with 1:2,000 diluted Alexa Fluor 488 and 555-conjugated secondary antibodies (Cell Signaling Technology, Inc.). Nuclei were labeled with DAPI from Beyotime Institute of Biotechnology, and visualization was carried out at x400 magnification using an Olympus fluorescence microscope at x200 magnification.

Tubular injury was assessed based on histopathological changes, including cell lysis, loss of brush border, and cast formation in renal tubules. A blinded examination was performed, and the percentage of injured tubules was scored as follows: 0 (no damage), 1 (<25%), 2 (25-50%), 3 (50-75%) and 4 (>75%). A total of 10 randomly selected fields were evaluated per mouse for quantification, and the mean score was calculated as the tubular injury score. The ImageJ 1.45 software (National Institutes of Health) was used to calculate the collagen volume fraction, that is, the percentage of the blue area (collagen) to the total area of each field. Randomly selected 10 fields of view per mouse kidney at a magnification of x200 were scored for quantification using an Olympus microscope and quantized with cellSens software (V3.2; cellSens) or an LSM880 laser scanning confocal microscope (Zeiss AG) system with a Plan-Apochromat 63x/1.4 objective and ZEN 2.3 software (Zeiss AG).

ImageJ 1.45 software (National Institutes of Health) was used to obtain the area (%) values for α-SMA staining (the percentage of the α-SMA positive green signal as a percentage of the total area of each field).

To detect cell apoptosis, a TUNEL apoptosis detection system (Promega Corporation) was utilized. The cellular nuclei were stained with DAPI for a duration of 3-5 min at ambient temperature, followed by inspection of the prepared sections under a fluorescence microscope at a magnification of x400. The number of TUNEL-positive cells was counted from 10 randomly selected fields of view per specimen in the outer medulla and kidney cortex regions (25).

Western blot analysis. Western blot assays were used to identify protein expression in kidney tissues and cells. Briefly, lysates containing whole cells, nuclei, or cytosolic extracts (with 10-50 mg of protein) were heated at 95˚C for 5 min in

Laemmli sample buffer (Bio-Rad Laboratories, Inc.). Proteins were then separated by polyacrylamide gel electrophoresis in acrylamide gels (8-15%) and transferred using a Bio-Rad western system to polyvinylidene difluoride membranes (Bio-Rad Laboratories, Inc.), which were immediately placed in 5% non-fat milk in Tris-buffered saline (TBS, 50 mM Tris, pH 7.6, 150 mM NaCl)-Tween (0.1% Tween20) buffer for blocking (1 h at 25˚C). Membranes were incubated overnight with antibodies against flavin-containing monooxygenase 1 (FMO1; cat. no. PA5-95285; Invitrogen; Thermo Fisher Scientific, Inc.; 1:1,000 dilution), FMO2 (cat. no. NBP1-85952; Novus Biologicals, LLC; 1:500), SMURF2 (cat. no. Ab53316; Abcam; 1:1,000), Histone3 (cat. no. Ab1791; Abcam; 1:1,000), phosphorylated SMAD3 (423/425) (cat. no. 9520; Cell Signaling Technology, Inc.; 1:1,000), SMAD3 (cat. no. 9523; Cell Signaling Technology, Inc.; 1:1,000), phosphorylated SMAD2 (465/467) (cat. no. 18338; Cell Signaling Technology, Inc.; 1:1,000), SMAD2 (cat. no. 8685; Cell Signaling Technology, Inc.; 1:1,000), Vimentin (cat. no. ab92547; Abcam; 1:1,000), FGF2 (cat. no. ab222932; Abcam; 1:1,000), PDGF (cat. no. ab178409; Abcam; 1:1,000), connective tissue growth factor (CTGF; cat. no. ab209780; Abcam; 1:1,000), α-SMA (cat. no. ab5694; Abcam; 1:5,000) and GAPDH (cat. no. CL594-60004; ProteinTech Group, Inc.; 1:20,000) at 4˚C. Membranes were then washed 3 times for 10 min in TBS-Tween buffer and incubated with a horseradish peroxidase-conjugated anti-mouse antibody (Servicebio; cat. no. GB23301; 1:10,000 dilution) or anti-rabbit antibody (Servicebio; cat. no. GB23303; 1:10,000 dilution) at 25˚C for 1 h. Films were scanned and signals detected using a Bio-Rad calibrated densitometer (Bio-Rad Laboratories, Inc.). ImageJ 1.45 software (National Institutes of Health) was used for densitometry analysis. Statistical analysis was performed using 3-5 biological replicates from 2-3 technical replicates.

Reverse transcription-quantitative (RT-q)PCR. Total RNA was extracted from whole kidney tissues or cells using TRIzol® reagent (Ambion; cat. no. 368711), according to the manufacturer's protocol. RNA reverse transcription reagents (Vazyme; cat. no. r323-01) were used to generate cDNA from 1 μg total RNA using an amplicon (Pcrsurecycler8800) according to the manufacturer's protocol. Real-time quantitative TaqMan PCR reagents (Vazyme; cat. no. q712-02) were employed, along with the TaqMan primers (Applied Biosystems; Thermo Fisher Scientific, Inc.) listed below. qPCR was performed on a real-time PCR instrument (Mx3005p), and data were analyzed using the $2^{-\Delta\Delta Cq}$ method for quantification (26). The sequences of the primers were as follows: Monocyte chemotactic protein 1 forward, 5'-CTG AGTTGACTCCTACTGTGGA-3' and reverse, 5'-TCTTCC CAGGGTCGATAAAGT-3'; IL-6 forward, 5'-CTGCAA GAGACTTCCATCCAG-3' and reverse, 5'-AGTGGTATA GACAGGTCTGTTGG-3'; Fgf2 forward, 5'-GCGACCCAC ACGTCAAACTA-3' and reverse, 5'-CCGTCCATCTTCCTT CATAGC-3'; Ccn2 forward, 5'-GGCCTCTTCTGCGAT TTCG-3' and reverse, 5'GCAGCTTGACCCTTCTCGG-3'; transforming growth factor β1 (TGF-β1) forward, 5'-CCA CCTGCAAGACCATCGAC-3' and reverse, 5'-CTGGCG AGCCTTAGTTTGGAC-3'; Pdgfb forward, 5'-TGCTGC ACAGAGACTCCGTA-3' and reverse, 5'-GATGAGCTT TCCAACTCGACTC-3'; and GAPDH forward, 5'-AAGTTC AACGGCACAGTCAA-3' and reverse, 5'-TCTCGCTCC TGGAAGATGG-3'.

Statistical analysis. Statistical analysis was performed using GraphPad Prism version 9.0.0 (Dotmatics), and the data are presented as the mean ± SEM. Normal distribution and homogeneity of variance were assessed using a Shapiro-Wilk test and Bartlett's test, respectively. For data that passed both normality and equality of variance, comparisons between two groups were performed using an unpaired 2-tailed Student's t-test, and multiple comparisons were analyzed using an ANOVA followed by a Tukey's post-hoc test. If not, the non-parametric Kruskal-Wallis test was used, followed by a Dunn's test. $P<0.05$ was considered to indicate a statistically significant difference.

Results

Dynamic expression of FMO2 in AKI-CKD transformation. To determine the alterations in the expression levels of the FMO family of enzymes during the process of AKI-CKD, the transcriptomic data of mouse kidney tissues were analyzed from the sham and IRI groups obtained from a public RNA sequencing database (GEO dataset GSE98622) (17). The FMO family consists of five subtypes (FMO1-5). Among them, FMO1 and FMO2 exhibited the highest abundance values in the kidneys (Fig. 1A and B). It is important to note that only FMO2 indicated a significant downregulation at the protein level in mouse kidney tissues following IRI (Fig. 1C). Consistent with the protein level changes, the mRNA levels of FMO2 were also lower in the IRI 24 h and IRI 14 day groups compared with those of the sham group (Fig. 1E). However, no significant differences were noted at the protein and mRNA levels of FMO1, which exhibited the highest abundance in the kidneys among the FMO subtypes (Fig. 1C and D). Immunostaining analysis was based on mouse kidney slices and the results further confirmed the significant downregulation of FMO2 expression in the IRI 24 h and IRI 14 day groups compared with the sham group. Therefore, the alteration of FMO2 expression may be dynamically associated with the occurrence of renal ischemic injury and fibrotic remodeling.

FMO2 alleviates ischemia-induced AKI. To investigate the role of FMO2 in renal AKI, mice were injected with lentivirus (LV)-FMO2 or a negative control (NC) 10 days prior to unilateral renal ischemia. Following 28 min of continuous ischemia and 24 h of reperfusion, the mice were euthanized (Fig. 2A). The mice treated with LV-FMO2 indicated a significant decrease in blood urea nitrogen and serum creatinine levels following IRI stimulation compared with the corresponding levels noted in the NC group (Fig. 2B and C). The extent of renal tissue damage was further assessed and examined using H&E, kidney injury molecule (KIM)-1, and TUNEL staining (Fig. 2D-F). It is important to note that the renal tubular injury score reached 2.9 following 28 min of ischemia and 24 h of reperfusion, while mice treated with LV-FMO2 exhibited less severe renal tubular injury with a score of 1.9 (Fig. 2G). Following IRI, the percentage of KIM-1-positive tubular cells in the LV-FMO2-treated group (57.6%) was significantly lower than that noted in the NC group

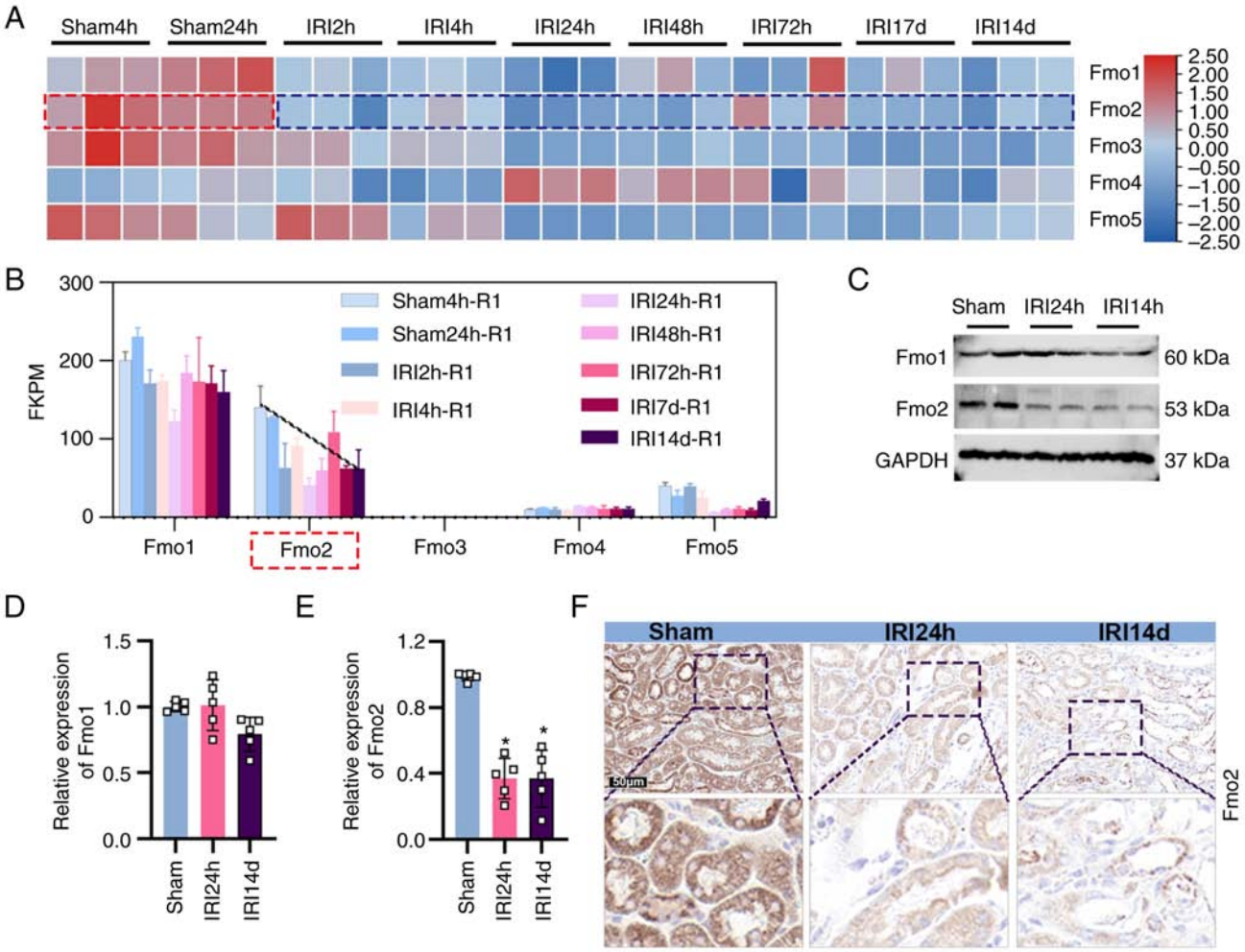

Figure 1. Kidney injury triggers downregulation of FMO2. (A) Normalized heatmap illustrating the dynamic changes in the transcriptome of the FMO family during the time period of 2 h to 14 days after renal IRI. The horizontal axis represents each sample, and the vertical axis represents each gene. Blue and red colors represent low and high values, respectively. (B) The transcriptome trend chart of time period of 2 h to 14 days after renal IRI. (C) Representative Western blot of FMO1 and FMO2. (D) Quantitative data showing the FMO1 protein abundance in mouse kidneys (n=5). *P<0.05 vs. sham. (E) Quantitative data showing the FMO2 protein abundance in mouse kidneys (n=5). *P<0.05 vs. sham. (F) Representative immunohistology images demonstrating kidney FMO2 expression in the sham group, and 24 h and 14 days after IRI (magnification, x400). FMO2, flavin-containing monooxygenase 2; IRI, ischemia-reperfusion injury; h, hour; d, day; FKPM, fragments per kilobase of exon model per million mapped fragments.

(38.4%, Fig. 2H). The LV-FMO2-treated mice had a significantly lower number of apoptotic cells (130/mm^2) compared with that of the NC group (98/mm^2, Fig. 2I). Following immunoblotting analysis, the levels of FMO2 were significantly higher in the LV-FMO2-treated mice compared with those of the LV-NC-treated mice (Fig. 2J). These results suggested that FMO2 may exert a protective effect during the injury phase of ischemic AKI.

Expression of FMO2 in the kidney prevents the development of fibrosis. To examine the impact of FMO2 on renal fibrosis following ischemia-reperfusion, the mice were injected with LV vectors containing LV-FMO2 or an NC into the kidney 10 days prior to unilateral left renal ischemia. The mice underwent 28 min of continuous ischemia, followed by unilateral right nephrectomy on the 13th day following reperfusion, and were euthanized on the 14th day (Fig. 3A). Following the removal of the right kidney, the levels of blood urea nitrogen and serum creatinine increased (Fig. 3B and C). Staining for vimentin (Fig. 3D), Masson's trichrome (Fig. 3E) and α-SMA (Fig. 3G) revealed significant ECM deposition in the renal tubulointerstitium on the 14th day following ischemia-reperfusion treatment (Fig. 3F). Furthermore, western blot analysis of and expression in the mouse kidneys (Fig. 3H-J) confirmed that overexpression of FMO2 attenuated renal dysfunction and fibrosis induced by IRI.

Expression of FMO2 reduces the infiltration of immune cells into the kidneys. Subsequent evaluation of the impact of FMO2 expression on immune cell infiltration was conducted. Immunohistochemical analysis using MPO staining indicated the presence of neutrophils, while F4/80 staining indicated the presence of macrophages. The expression of FMO2 limited the inflammatory infiltration of neutrophils (Fig. 4A and B) and macrophages (Fig. 4C and D) compared with that noted in the IRI 14-day NC group. In addition, qPCR analysis demonstrated that the expression of FMO2 suppressed the expression levels of pro-inflammatory cytokines, such as IL-6, chemokine ligand 1 and monocyte chemoattractant protein 1 (Fig. 4E and G).

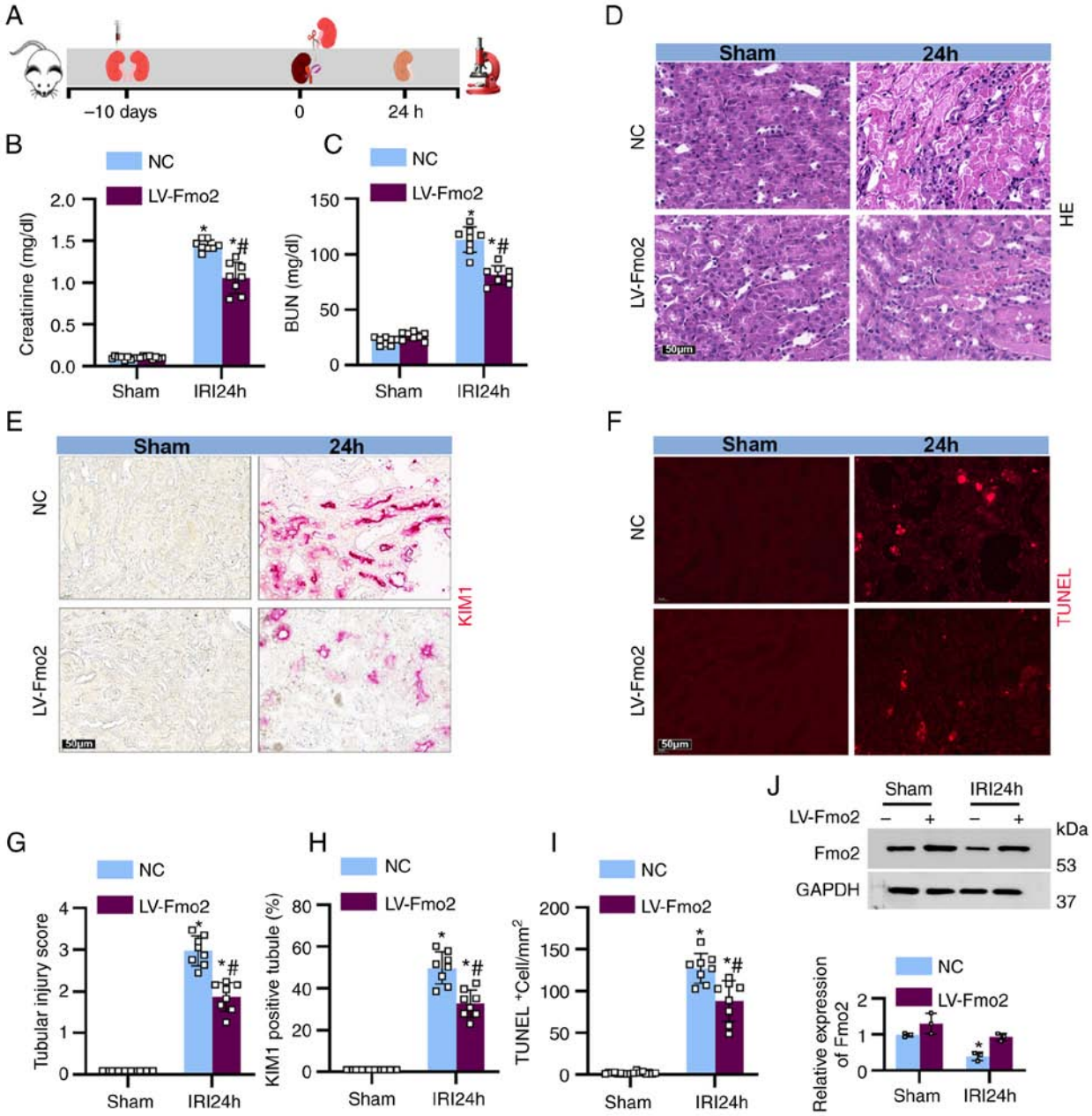

Figure 2. Targeted FMO2 expression alleviates ischemia-induced acute kidney injury. LV harboring FMO2 was injected into the kidney 10 days before unilateral left renal ischemia was clamped for 28 min. A right nephrectomy was performed prior to reperfusion. The serum and kidneys were collected 24 h after nephrectomy for further analysis. (A) Schematic diagram of the experimental procedure. (B) Serum creatinine 24 h after reperfusion. (C) Blood urea nitrogen levels are shown. (D) Representative images of hematoxylin and eosin staining. (E) Representative images of KIM-1 immunohistochemistry. (F) Representative images of TUNEL staining to show apoptosis in kidney tissues. (G) Quantification of the tubular damage score. (H) Quantitative analysis of KIM-1 positive tubules. (I) Quantification of the TUNEL staining (magnification, x400) (n=8). *P<0.05 vs. sham; #P<0.05 vs. NC-IRI24h group. (J) Representative western blot and quantitative data showing the FMO2 protein abundance in sham or IRI- treated kidneys from (LV)FMO2 or (NC) mice. (n=3). FMO2, flavin-containing monooxygenase 2; IRI, ischemia-reperfusion injury; h, hour; d, day; NC, negative control; LV, lentivirus.

In vitro, decreased expression of FMO2 in BUMPT cells diminishes the effect of TGF-β. The *in vitro* data of the present study suggested that the expression of FMO2 in tubular cells exerted anti-fibrotic effects. In BUMPT cells cultured under basal conditions without TGF-β stimulation, minimal expression of vimentin and α-SMA was observed. However, significant expression of vimentin and α-SMA was observed in BUMPT cells following TGF-β stimulation. The expression of FMO2 effectively prevented the responsiveness of BUMPT cells to TGF-β stimulation (Fig. 5A and B). Furthermore, fluorescence co-staining of FMO2 and α-SMA revealed that TGF-β stimulation led to a decrease in FMO2 expression and an increase in α-SMA expression (Fig. 5C). qPCR results demonstrated that the expression of FMO2 suppressed the expression levels of fibrotic factors induced by TGF-β, including α-SMA, TGF-β1, PDGF-β, and cellular communication network factor 2 (Fig. 5D-G).

Expression of FMO2 reduces the paracrine secretion of pro-fibrotic factors from BUMPT cells, inhibiting the activation of fibroblasts. The results indicated that the conditioned medium from TGF-β-induced BUMPT cells exerted an activating effect on fibroblasts. The medium exposed to BUMPT

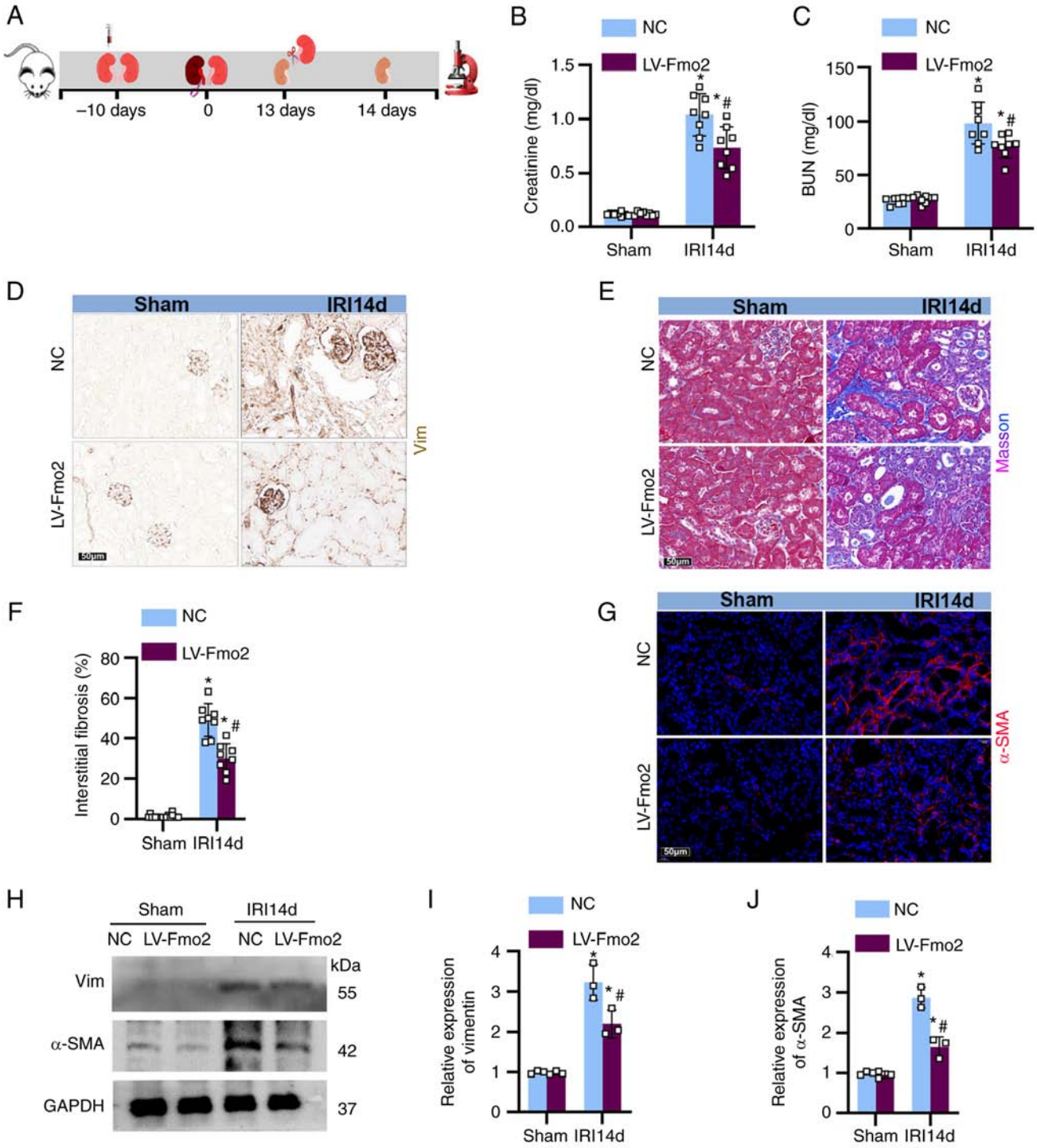

Figure 3. Targeting the expression of FMO2 can attenuate the progression of renal fibrosis. LV harboring FMO2 was injected into the kidney 10 days before unilateral left renal ischemia was clamped for 28 min. A right nephrectomy was performed on day 13 of reperfusion. The serum and kidneys were collected 24 h after nephrectomy for further analysis. (A) Schematic diagram of the experimental procedure. (B) Serum creatinine 14 days after reperfusion. (C) Blood urea nitrogen levels are shown. (D) Representative images of Vimentin immunohistochemical staining. (E) Representative graphs of Masson staining from the sham and IRI14d groups. (F) Quantitative analysis of renal fibrosis. (G) Representative graphs of α-SMA fluorescence staining. (H) Representative immunoblot for α-SMA or Vimentin protein levels in mouse kidneys. (I) Quantitative data showing the Vimentin protein abundance in mouse kidneys (n=3). *P<0.05 vs. sham; #P<0.05 vs. NC-IRI24h group. (J) Quantitative data showing the α-SMA protein abundance in mouse kidneys (n=3). *P<0.05 vs. sham; #P<0.05 vs. NC-IRI24h group. FMO2, flavin-containing monooxygenase 2; IRI, ischemia-reperfusion injury; h, hour; d, day; NC, negative control; LV, lentivirus; Vim, vimentin.

cells containing TGF-β exhibited a significant increase in the levels of paracrine fibrotic factors, such as FGF2, PDGF, and CTGF. The expression of FMO2 partially alleviated the paracrine secretion of FGF2 and other factors (Fig. 6A). Conditioned medium from TGF-β-treated BUMPT cells was collected, centrifuged, and subsequently used to culture NRK-49F cells (Fig. 6B). Immunofluorescence staining of NRK-49F cells revealed that the conditioned medium from LV-FMO2-treated BUMPT cells exhibited a noticeable reduction in the expression levels of α-SMA and vimentin (Fig. 6C).

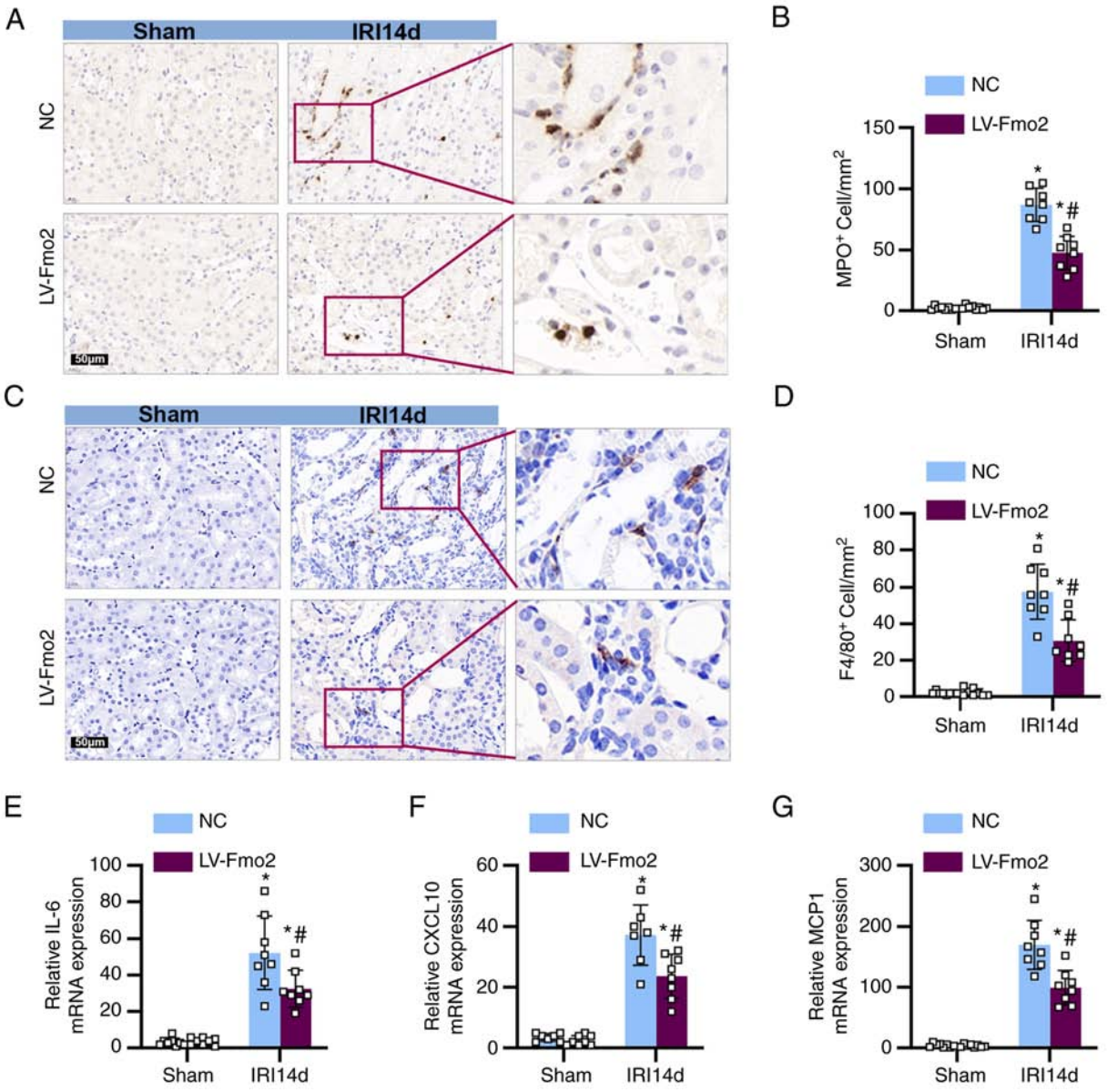

Figure 4. Targeting the expression of FMO2 attenuates immune cell infiltration into the kidneys. (A) Representative immunohistochemistry graphs of renal sections with MPO staining. (B) Quantitative analysis of MPO-positive tubular epithelial cells. (C) Representative F4/80 immunohistochemistry graphs of renal sections. (D) Quantitative analysis of F4/80 positive tubular epithelial cells. (E) mRNA expression of IL-6 in kidney homogenates from mice 14 day after I/R and sham (n=8). (F) mRNA expression of CXCL10 in kidney homogenates from mice 14 day after I/R and sham (n=8). (G) mRNA expression of MCP-1 in kidney homogenates from mice 14 day after I/R and sham (n=8). *P<0.05 vs. sham; #P<0.05 vs. NC-IRI24h group. FMO2, flavin-containing monooxygenase 2; IRI, ischemia-reperfusion injury; MPO, myeloperoxidase; FMO2, flavin-containing monooxygenase 2; NC, negative control; LV, lentivirus.

FMO2 inhibits the phosphorylation of SMAD2/3 by promoting the translocation of SMURF2 to the nucleus. Due to the cytoplasmic localization of FMO2, this enzyme is unlikely to directly participate in transcriptional gene regulation. Therefore, the transcriptional post-effects mediated by FMO2 and its subsequent anti-fibrotic actions mediated via inhibition of SMAD2/3 phosphorylation were examined. SMURF2, an E3 ubiquitin ligase, exhibits specific activity towards phosphorylated SMAD2/3 in the nucleus (27) and plays a crucial role in the negative regulation of the TGF-β signaling pathway. Initially, co-immunofluorescence staining of FMO2 (green) and SMURF2 (red) was performed in the kidney tissues of IRI 14 day mice, revealing nuclear translocation of SMURF2 under conditions of high FMO2 expression (Fig. 7A). The elevated expression of FMO2 in BUMPT cells significantly reduced the levels of phosphorylated SMAD2/3, as determined by its phosphorylation state (Fig. 7B). Furthermore, by using nuclear protein extraction and immunoblotting, it was confirmed that the expression of FMO2 promoted the translocation of SMURF2 from the cytoplasm to the nucleus (Fig. 7C). These data suggest that FMO2 ultimately facilitates the nuclear translocation of SMURF2, by regulating its expression and leads to inhibition of TGF-β signaling (Fig. 7D).

Discussion

The present study provides three primary conclusions. First, the expression levels of FMO2 were evaluated, which is a member of the FMO gene family, that are abundantly expressed in the kidney, and dynamically associated with

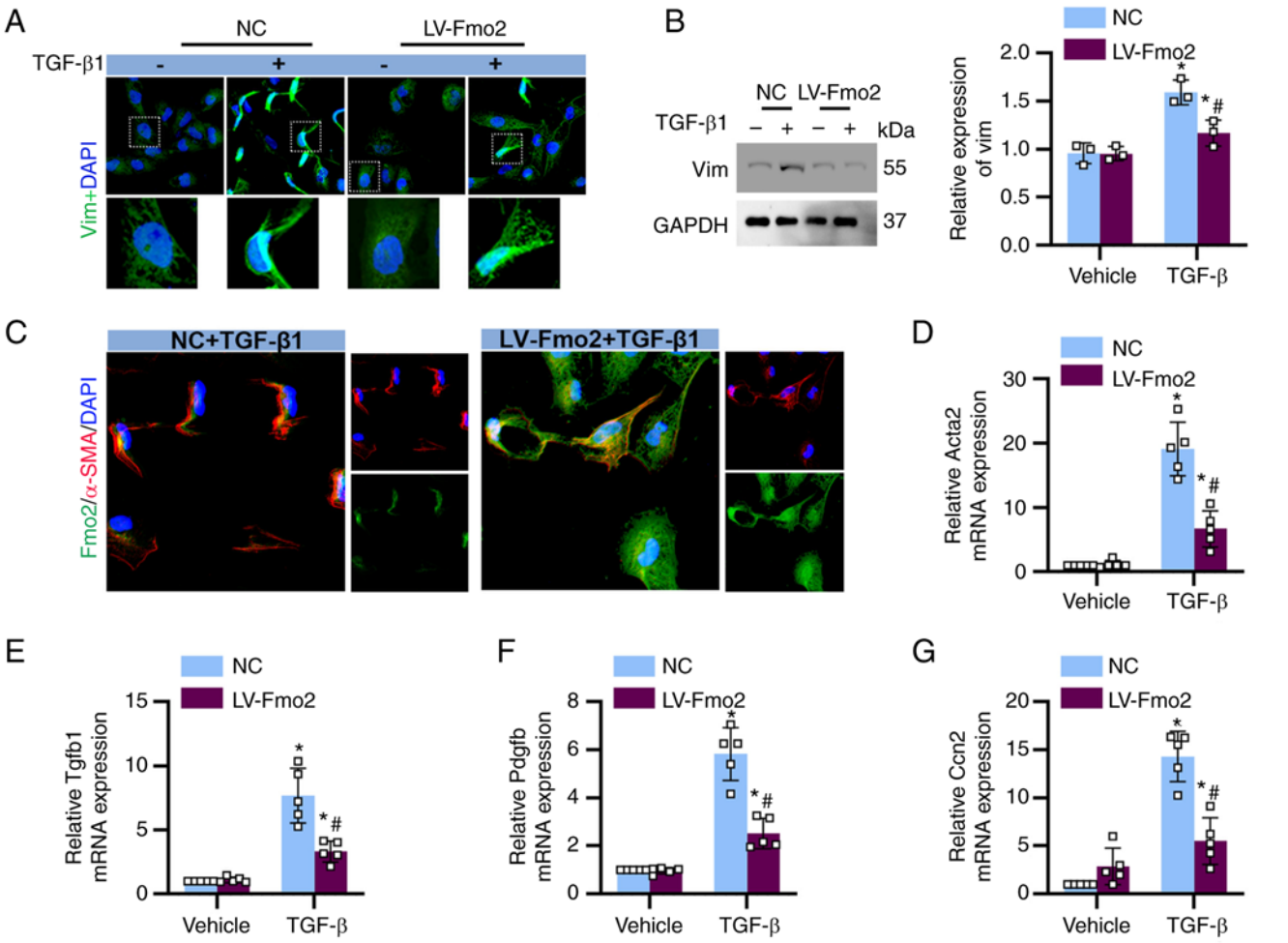

Figure 5. The expression of FMO2 reduces the impact of TGF-β on BUMPT cells. (A) Cellular morphology and vimentin expression profile observed using immunofluorescence staining. (B) Representative immunoblot of α-SMA and vimentin protein levels in BUMPT cells (n=3). *P<0.05 vs. vehicle; #P<0.05 vs. NC-TGF-β group. (C) Representative immunofluorescence images of BUMPT cells stained with anti-FMO2 (green) and anti-α-SMA (red) antibodies and DAPI (blue). (D) mRNA expression levels of Acta2 in BUMPT cells (n=5). (E) mRNA expression levels of Tgfb1 in BUMPT cells (n=5). (F) mRNA expression levels of Pdgfb in BUMPT cells (n=5). (G) mRNA expression levels of Ccn2 in BUMPT cells (n=5). *P<0.05 vs. vehicle; #P<0.05 vs. NC-TGF-β group. FMO2, flavin-containing monooxygenase 2; BUMPT, Boston University mouse proximal tubule; NC, negative control.

renal ischemic injury and fibrotic remodeling. Overexpression of FMO2 alleviated renal ischemia-reperfusion-induced AKI, renal fibrosis, and immune cell infiltration into the kidney. Second, FMO2 overexpression not only effectively blocked TGF-β-induced tubular cell fibrosis but also inhibited the activation of aberrant tubular cell-derived paracrine fibrogenic factors on fibroblasts. Thirdly, FMO2 negatively regulated TGF-β-induced SMAD2/3 activation by promoting the expression and nuclear translocation of SMURF2. Therefore, FMO2 emerges as a previously unidentified modulator of TGF-β signaling, playing a conserved key role in fibroblast activation and fibrotic remodeling following injury.

The enzymes of the FMO family are primarily present in animals and microorganisms. The canonical function of most FMO gene family members involves enzymatic activity-dependent cellular detoxification (19). Unexpectedly, however, the FMO2-mediated suppression of TGF-β activity is independent of its enzymatic activity. While the nonenzymatic FMO2 isoform has been reported in mammals (27,28), its biological role has never been clearly elucidated. They participate in the metabolism of various substrates, including drugs and toxins, and are involved in specific biological processes (29). The members of the FMO family are predominantly expressed in tissues, such as the liver and kidneys, exhibiting structural and functional diversity. The FMO family consists of five subtypes (FMO1-5), each potentially differing in tissue distribution, catalytic properties, and substrate specificity; these enzymes play important roles in drug metabolism (27). By using analysis of transcriptomic data following renal IRI, it was discovered that the expression of one member of the FMO gene family, FMO2, was highly enriched in tubular cells and dynamically associated with renal injury and fibrotic remodeling. However, previous studies have shown that FMO2-mediated inhibition of TGF-β activity is independent of its enzymatic activity (18). Although non-enzymatic isoforms of FMO2 have been reported in humans and rats (30-32) and have been shown to influence the lifespan of the nematode Caenorhabditis elegans (33), their biological roles remain unclear. It is important to note that the downregulation of FMO2 expression in renal tubular cells is a conserved molecular characteristic in response to injury and TGF-β stimulation, while FMO2 inactivation is sufficient to promote the induction of fibrosis and

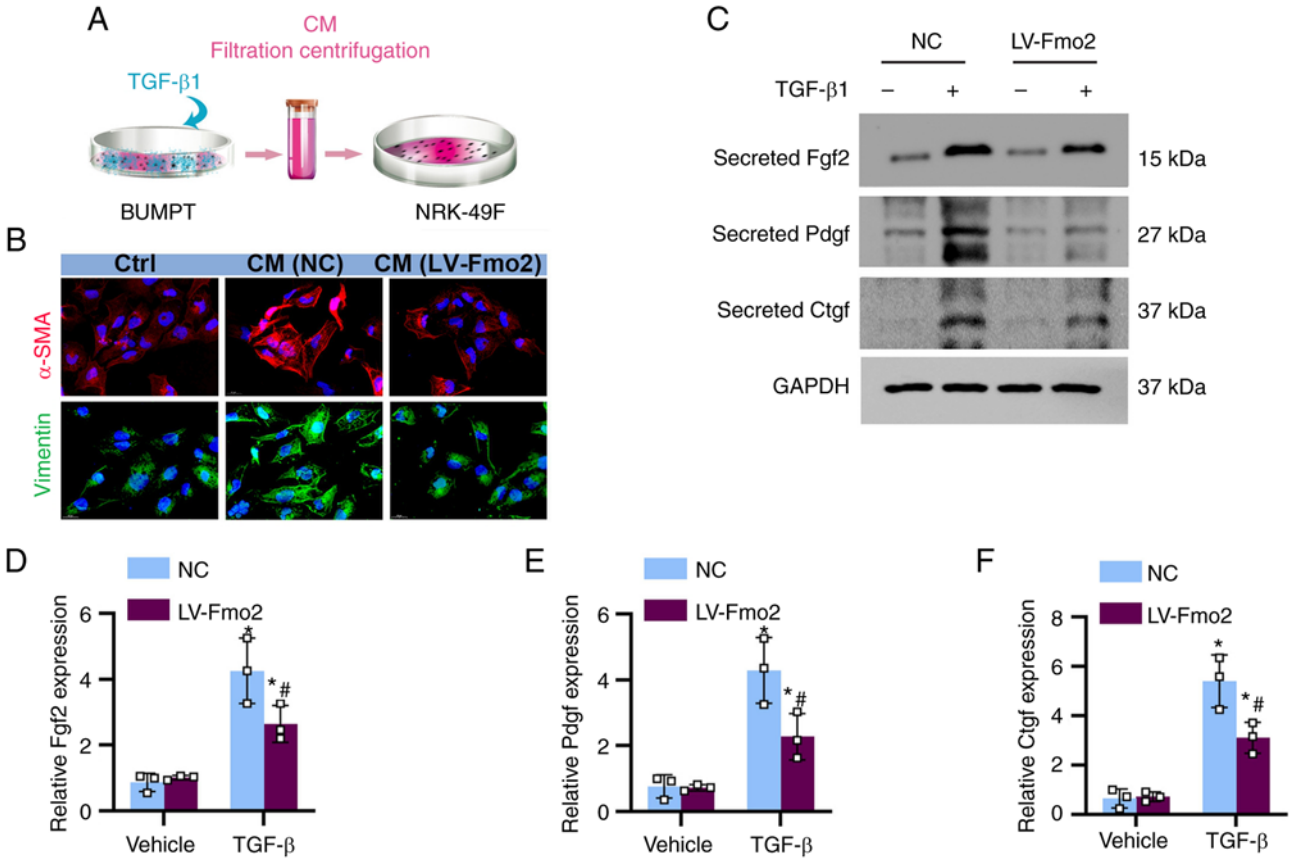

Figure 6. BUMPT cells secrete fibrosis-promoting factors that stimulate fibroblast activation. (A) Conditioned medium from TGF-β-treated BUMPT cells was collected, centrifuged, and used to culture NRK-49F (model diagram). (B) Immunofluorescence staining of α-SMA and vimentin expression in NRK-49F cells. (C) Immunoblot analysis of matrix cell proteins FGF2, PDGF, and CTGF. (D) Quantitative data showing the FGF2 protein abundance in NRK-49F cells (n=3). *P<0.05 vs. respective vehicle; #P<0.05 vs. NC with TGF-β. (E) Quantitative data showing the PDGF protein abundance in NRK-49F cells (n=3). *P<0.05 vs. respective vehicle; #P<0.05 vs. NC with TGF-β. (F) Quantitative data showing the CTGF protein abundance in NRK-49F cells (n=3). *P<0.05 vs. respective vehicle; #P<0.05 vs. NC with TGF-β. NC, negative control; BUMPT, Boston University mouse proximal tubule; FMO2, flavin-containing monooxygenase 2; NC, negative control.

renal dysfunction. By contrast, overexpression of FMO2 alleviated renal ischemia-reperfusion-induced AKI, renal fibrosis, and immune cell infiltration into the kidney. Therefore, FMO2 emerges as a previously unidentified modulator in the progression from AKI to CKD, playing a crucial role in tubular cell fibroblast transition, fibroblast activation, and interstitial fibrotic remodeling following renal injury.

Impaired adaptive repair of the kidney following AKI is a fundamental pathophysiological mechanism leading to renal fibrosis and progression to CKD. Defective repair of proximal tubular epithelial cells is a key factor in the progression from AKI to CKD. In the early stages of injury, surviving tubular cells mount an adaptive response, undergoing dedifferentiation and proliferation to repair the damaged renal tubules (34). However, severe AKI injury can result in aberrant repair of tubular cells, leading to the production and secretion of various cytokines, growth factors, pro-inflammatory molecules, and pro-fibrotic molecules (10). The increased levels of these bioactive molecules play a role in both autocrine functions, which are necessary for tubular cell regeneration via dedifferentiation, migration, and proliferation, and paracrine functions, recruiting circulating leukocytes and activating interstitial cells, such as fibroblasts (35). During the AKI-CKD process, aberrant paracrine secretion of fibrotic factors by tubular cells, such as CTGF, PDGF and FGF2, stimulates adjacent myofibroblasts to produce ECM components, which in turn activates the fibroblasts (36). However, the molecular mechanisms involved in the regulation of impaired tubular cell paracrine secretion of fibrotic factors are not fully understood. Previous studies have focused on the abnormal metabolic adaptation of tubular cells in AKI, proposing that disrupted adaptive energy metabolism has a crucial role in promoting CKD progression (37,38).

In the present study, a unilateral ischemia-reperfusion model was used to characterize the role of FMO2 in AKI-CKD, and validation experiments were conducted in immortalized cell lines. While data from these models consistently demonstrate the beneficial effects of FMO2 in treating renal fibrosis and CKD, they are not without limitations. The main limitation is the lack of verification in FMO2 knockout mice. Therefore, although the data from this model suggest the involvement of FMO2 in the development and progression of renal fibrosis, they do not exclude the contribution of potential other detrimental factors in the absence of FMO2; moreover, they do not specify the specific renal segment in which FMO2 inhibits fibrotic reactions. Future studies are required to elucidate the role of FMO2 in the AKI-to-CKD transition. Another limitation is that FMO2 is not solely expressed by

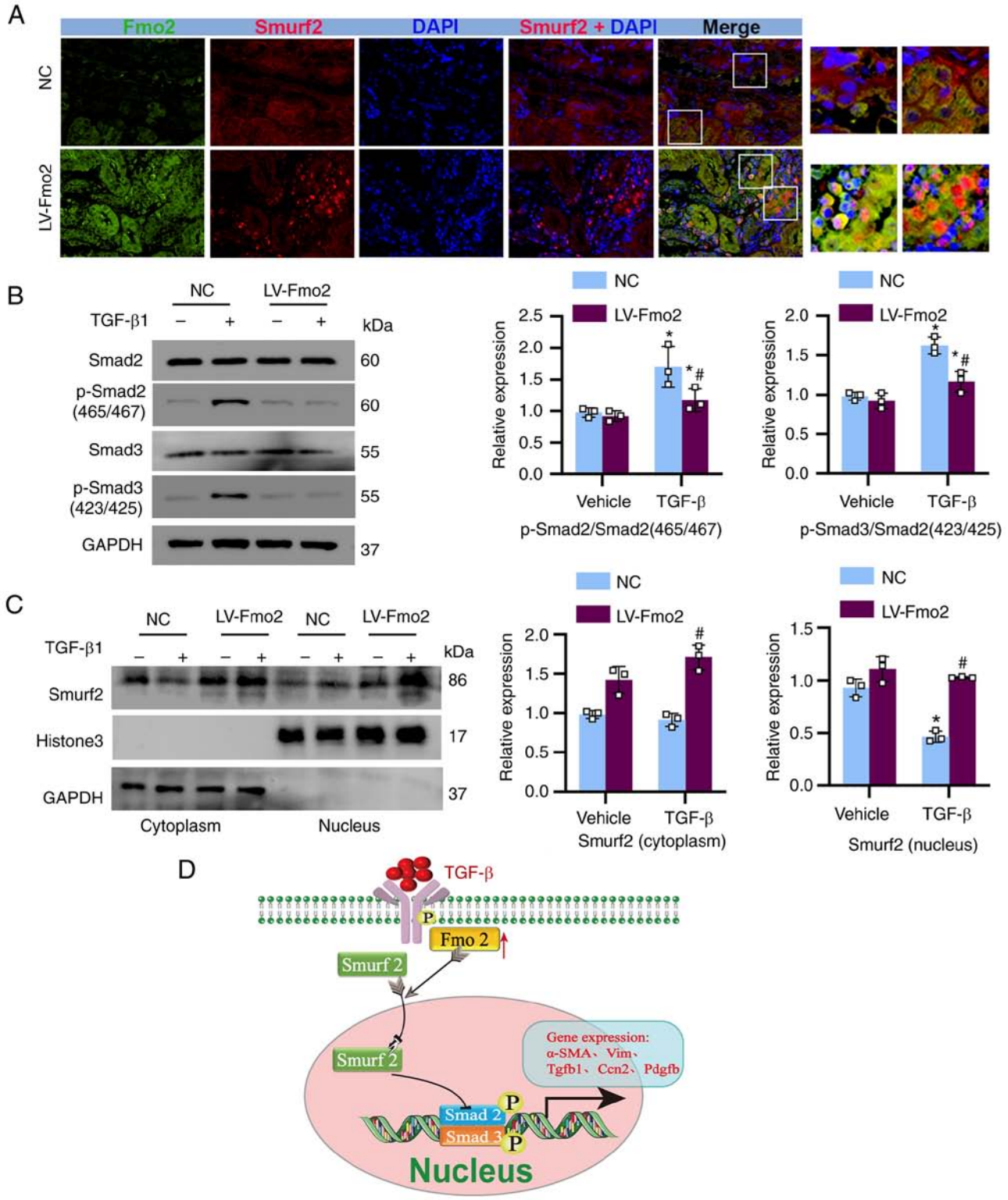

Figure 7. FMO2 inhibits the phosphorylation of SMAD2/3 via promoting SMURF2 nuclear translocation. (A) Immunofluorescence colocalization of SMURF2 (red) with FMO2 (green) in kidney tissue at 14 days of reperfusion (magnification, x400). (B) Immunoblot and quantitative analysis revealed the alterations in phosphorylation of SMAD2/3 in FMO2-expressing BUMPT cells (n=3). *P<0.05 vs. respective vehicle; #P<0.05 vs. NC with TGF-β. (C) Increased nuclear translocation of SMURF2 was observed in BUMPT cells following FMO2 overexpression under TGF-β stimulation as shown in immunoblot and quantitative from the cytosolic and the nuclear fractions as indicated (n=3). *P<0.05 vs. respective vehicle; #P<0.05 vs. NC with TGF-β. (D) The schematic diagram illustrates the regulatory role of FMO2 in the phosphorylation of SMAD2/3 and renal fibrosis through SMURF2. FMO2, flavin-containing monooxygenase 2; NC, negative control; SMURF2, SMAD ubiquitination regulatory factor 2; BUMPT, Boston University mouse proximal tubule.

tubular cells. It is also expressed in other tubular segments and certain non-tubular cells. Future research should determine the role of FMO2 in other cell populations within the kidney. In the present study, conditioned media were collected from TGF-β-stimulated renal tubular cells, which were used to stimulate fibroblasts to secrete ECM. However, the secretion

of ECM was significantly reduced when renal tubular cells were transfected with LV-expressing FMO2, suggesting the presence of other active substances in the conditioned media (following FMO2 overexpression) that play important roles (Fig. 6). Therefore, the findings of the present study aid the confirmation of the specific effects of the FMO2 gene on renal tubular cells. Although the *in vivo* and *in vitro* models in the present study have certain limitations, when considered together, the data from these models suggest specific roles of FMO2 in AKI-CKD. Furthermore, a novel function of FMO2 was discovered in the kidney as a signaling regulator and not as a metabolic enzyme; the FMO2-SMURF2-mediated negative regulatory circuitry modulates the phosphorylation and activation of SMAD2/3 in response to TGF-β signaling in fibroblasts (27,39).

In conclusion, the present study demonstrated that FMO2 can regulate maladaptive repair and renal fibrosis following AKI through the expression and nuclear translocation of SMURF2. FMO2 not only effectively inhibited TGF-β-induced tubular cell fibrosis but also suppressed the abnormal paracrine secretion of fibrogenic factors by tubular cells. The regulation of fibrosis mediated by FMO2 holds significant therapeutic implications by inhibiting the transition from AKI to CKD.

During the transition from AKI to CKD, FMO2 modulates tubular cell fibrogenesis and paracrine secretion via SMURF2, thereby impacting the outcome of this process.

Acknowledgements

Not applicable.

Funding

This work was supported by the National Natural Science Foundation of China (grant no. NSFC82100340) and the Open Project of Henan International Joint Laboratory of Prevention and Treatment of Pediatric Diseases (grant no. EKB202203).

Availability of data and materials

The datasets used and/or analyzed during the present study are available from the corresponding author on reasonable request.

Authors' contributions

LW, HZ, JH and LS confirm the authenticity of all the raw data. LS contributed to the conception of the study. LW, HZ and JH performed the experiments. HZ, LW and JH performed the analysis. HZ and LW drafted the manuscript. LS reviewed the manuscript. All authors have read and approved the final manuscript.

Ethics approval and consent to participate

All animal experiments were performed in compliance with the Animal Management Regulations of the Ministry of Health of the P.R. China and approved by the Ethics Committee of the Children's Hospital Affiliated to Zhengzhou University (approval no. 2023-K-074).

Patient consent for publication

Not applicable.

Competing interests

The authors declare that they have no competing interests.

References

1. Hoste EAJ, Kellum JA, Selby NM, Zarbock A, Palevsky PM, Bagshaw SM, Goldstein SL, Cerdá J and Chawla LS: Global epidemiology and outcomes of acute kidney injury. Nat Rev Nephrol 14: 607-625, 2018.
2. James MT, Bhatt M, Pannu N and Tonelli M: Long-term outcomes of acute kidney injury and strategies for improved care. Nat Rev Nephrol 16: 193-205, 2020.
3. Turgut F, Awad AS and Abdel-Rahman EM: Acute kidney injury: Medical causes and pathogenesis. J Clin Med 12: 375, 2023.
4. Zhao ZB, Marschner JA, Iwakura T, Li C, Motrapu M, Kuang M, Popper B, Linkermann A, Klocke J, Enghard P, *et al*: Tubular epithelial cell HMGB1 promotes AKI-CKD transition by sensitizing cycling tubular cells to oxidative stress: A rationale for targeting HMGB1 during AKI recovery. J Am Soc Nephrol 34: 394-411, 2023.
5. Kurata Y and Nangaku M: Use of antibiotics as a therapeutic approach to prevent AKI-to-CKD progression. Kidney Int 104: 418-420, 2023.
6. Patidar KR, Naved MA, Grama A, Adibuzzaman M, Aziz Ali A, Slaven JE, Desai AP, Ghabril MS, Nephew L, Chalasani N and Orman ES: Acute kidney disease is common and associated with poor outcomes in patients with cirrhosis and acute kidney injury. J Hepatol 77: 108-115, 2022.
7. Shi L, Song Z, Li Y, Huang J, Zhao F, Luo Y, Wang J, Deng F, Shadekejiang H, Zhang M, *et al*: MiR-20a-5p alleviates kidney ischemia/reperfusion injury by targeting ACSL4-dependent ferroptosis. Am J Transplant 23: 11-25, 2023.
8. Mansour SG, Bhatraju PK, Coca SG, Obeid W, Wilson FP, Stanaway IB, Jia Y, Thiessen-Philbrook H, Go AS, Ikizler TA, *et al*: Angiopoietins as prognostic markers for future kidney disease and heart failure events after acute kidney injury. J Am Soc Nephrol 33: 613-627, 2022.
9. Gewin LS: Renal fibrosis: Primacy of the proximal tubule. Matrix Biol 68-69: 248-262, 2018.
10. Sheng L and Zhuang S: New insights into the role and mechanism of partial epithelial-mesenchymal transition in kidney fibrosis. Front Physiol 11: 569322, 2020.
11. Xu C, Hong Q, Zhuang K, Ren X, Cui S, Dong Z, Wang Q, Bai X and Chen X: Regulation of pericyte metabolic reprogramming restricts the AKI to CKD transition. Metabolism 145: 155592, 2023.
12. Lewis MP, Fine LG and Norman JT: Pexicrine effects of basement membrane components on paracrine signaling by renal tubular cells. Kidney Int 49: 48-58, 1996.
13. Kuppe C, Ibrahim MM, Kranz J, Zhang X, Ziegler S, Perales-Paton J, Jansen J, Reimer KC, Smith JR, Dobie R, *et al*: Decoding myofibroblast origins in human kidney fibrosis. Nature 589: 281-286, 2021.
14. Gong H, Zheng C, Lyu X, Dong L, Tan S and Zhang X: Inhibition of Sirt2 alleviates fibroblasts activation and pulmonary fibrosis via Smad2/3 pathway. Front Pharmacol 12: 756131, 2021.
15. Khalil H, Kanisicak O, Prasad V, Correll RN, Fu X, Schips T, Vagnozzi RJ, Liu R, Huynh T, Lee SJ, *et al*: Fibroblast-specific TGF-β-Smad2/3 signaling underlies cardiac fibrosis. J Clin Invest 127: 3770-3783, 2017.
16. Yang Q, Ren GL, Wei B, Jin J, Huang XR, Shao W, Li J, Meng XM and Lan HY: Conditional knockout of TGF-βRII/Smad2 signals protects against acute renal injury by alleviating cell necroptosis, apoptosis and inflammation. Theranostics 9: 8277-8293, 2019.
17. Liu J, Kumar S, Dolzhenko E, Alvarado GF, Guo J, Lu C, Chen Y, Li M, Dessing MC, Parvez RK, *et al*: Molecular characterization of the transition from acute to chronic kidney injury following ischemia/reperfusion. JCI Insight 2: e94716, 2017.
18. Ni C, Chen Y, Xu Y, Zhao J, Li Q, Xiao C, Wu Y, Wang J, Wang Y, Zhong Z, *et al*: Flavin containing monooxygenase 2 prevents cardiac fibrosis via CYP2J3-SMURF2 axis. Circ Res: July 5, 2022 (Epub ahead of print).

19. Krueger SK, Williams DE, Yueh MF, Martin SR, Hines RN, Raucy JL, Raucy JL, Dolphin CT, Shephard EA and Phillips IR: Genetic polymorphisms of flavin-containing monooxygenase (FMO). Drug Metab Rev 34: 523-532, 2002.
20. Siddens LK, Henderson MC, Vandyke JE, Williams DE and Krueger SK: Characterization of mouse flavin-containing monooxygenase transcript levels in lung and liver, and activity of expressed isoforms. Biochem Pharmacol 75: 570-579, 2008.
21. Hsu DZ, Chu PY, Li YH, Chandrasekaran VR and Liu MY: Role of flavin-containing-monooxygenase-dependent neutrophil activation in thioacetamide-induced hepatic inflammation in rats. Toxicology 298: 52-58, 2012.
22. Zhang J, Chaluvadi MR, Reddy R, Motika MS, Richardson TA, Cashman JR and Morgan ET: Hepatic flavin-containing monooxygenase gene regulation in different mouse inflammation models. Drug Metab Dispos 37: 462-468, 2009.
23. Ding H, Li J, Li Y, Yang M, Nie S, Zhou M, Yang X, Liu Y and Hou FF: MicroRNA-10 negatively regulates inflammation in diabetic kidney via targeting activation of the NLRP3 inflammasome. Mol Ther 29: 2308-2320, 2021.
24. Shi L, Song Z, Li C, Deng F, Xia Y, Huang J, Wu X and Zhu J: HDAC6 inhibition alleviates ischemia- and Cisplatin-induced acute kidney injury by promoting autophagy. Cells 11: 3951, 2022.
25. Moore CL, Savenka AV and Basnakian AG: TUNEL assay: A powerful tool for kidney injury evaluation. Int J Mol Sci 22: 412, 2021.
26. Livak KJ and Schmittgen TD: Analysis of relative gene expression data using real-time quantitative PCR and the 2(-Delta Delta C(T)) method. Methods 25: 402-408, 2001.
27. Lin X, Liang M and Feng XH: Smurf2 is a ubiquitin E3 ligase mediating proteasome-dependent degradation of Smad2 in transforming growth factor-beta signaling. J Biol Chem 275: 36818-36822, 2000.
28. Choi HS, Bhat A, Howington MB, Schaller ML, Cox RL, Huang S, Beydoun S, Miller HA, Tuckowski AM, Mecano J, *et al*: FMO rewires metabolism to promote longevity through tryptophan and one carbon metabolism in C. elegans. Nat Commun 14: 562, 2023.
29. Krueger SK, Vandyke JE, Williams DE and Hines RN: The role of flavin-containing monooxygenase (FMO) in the metabolism of tamoxifen and other tertiary amines. Drug Metab Rev 38: 139-147, 2006.
30. Bailleul G, Yang G, Nicoll CR, Mattevi A, Fraaije MW and Mascotti ML: Evolution of enzyme functionality in the flavin-containing monooxygenases. Nat Commun 14: 1042, 2023.
31. Whetstine JR, Yueh MF, McCarver DG, Williams DE, Park CS, Kang JH, Cha YN, Dolphin CT, Shephard EA, Phillips IR and Hines RN: Ethnic differences in human flavin-containing monooxygenase 2 (FMO2) polymorphisms: Detection of expressed protein in African-Americans. Toxicol Appl Pharmacol 168: 216-224, 2000.
32. Hugonnard M, Benoit E, Longin-Sauvageon C and Lattard V: Identification and characterization of the FMO2 gene in Rattus norvegicus: A good model to study metabolic and toxicological consequences of the FMO2 polymorphism. Pharmacogenetics 14: 647-655, 2004.
33. Leiser SF, Miller H, Rossner R, Fletcher M, Leonard A, Primitivo M, Rintala N, Ramos FJ, Miller DL and Kaeberlein M: Cell nonautonomous activation of flavin-containing monooxygenase promotes longevity and health span. Science 350: 1375-1378, 2015.
34. Liu BC, Tang TT, Lv LL and Lan HY: Renal tubule injury: A driving force toward chronic kidney disease. Kidney Int 93: 568-579, 2018.
35. Garimella PS, Katz R, Waikar SS, Srivastava A, Schmidt I, Hoofnagle A, Palsson R, Rennke HG, Stillman IE, Wang K, *et al*: Kidney tubulointerstitial fibrosis and tubular secretion. Am J Kidney Dis 79: 709-716, 2022.
36. Livingston MJ, Shu S, Fan Y, Li Z, Jiao Q, Yin XM, Venkatachalam MA and Dong Z: Tubular cells produce FGF2 via autophagy after acute kidney injury leading to fibroblast activation and renal fibrosis. Autophagy 19: 256-277, 2023.
37. Li Z, Lu S and Li X: The role of metabolic reprogramming in tubular epithelial cells during the progression of acute kidney injury. Cell Mol Life Sci 78: 5731-5741, 2021.
38. Xu P, Chen C, Zhang Y, Dzieciatkowska M, Brown BC, Zhang W, Xie T, Abdulmalik O, Song A, Tong C, *et al*: Erythrocyte transglutaminase-2 combats hypoxia and chronic kidney disease by promoting oxygen delivery and carnitine homeostasis. Cell Metab 34: 299-316.e6, 2022.
39. Zhang Z, Fan Y, Xie F, Zhou H, Jin K, Shao L, Shi W, Fang P, Yang B, van Dam H, *et al*: Breast cancer metastasis suppressor OTUD1 deubiquitinates SMAD7. Nat Commun 8: 2116, 2017.